Biosensors and Bioelectronics 216 (2022) 114639

Contents lists available at ScienceDirect

Biosensors and Bioelectronics

journal homepage: www.elsevier.com/locate/bios

Highly sensitive protein detection by aptamer-based single-molecule kinetic fingerprinting

Tanmay Chatterjee [a], Alexander Johnson-Buck [b,**], Nils G. Walter [a,*]

[a] Single Molecule Analysis Group, Department of Chemistry, University of Michigan, Ann Arbor, Michigan, 48109, United States
[b] aLight Sciences, Inc., 333 Jackson Plaza Suite 460, Ann Arbor, Michigan, 48103, United States

ARTICLE INFO

Keywords:
Single molecule fluorescence microscopy
Kinetic fingerprinting
Protein biomarkers
Aptamer
Analyte detection
Sensitivity

ABSTRACT

Sensitive assays of protein biomarkers play critical roles in clinical diagnostics and biomedical research. Such assays typically employ immunoreagents such as monoclonal antibodies that suffer from several drawbacks, including relatively tedious production, significant batch-to-batch variability, and challenges in site-specific, stoichiometric modification with fluorophores or other labels. One proposed alternative to such immunoreagents, nucleic acid aptamers generated by systematic evolution of ligand by exponential enrichment (SELEX), can be chemically synthesized with much greater ease, precision, and reproducibility than antibodies. However, most aptamers exhibit relatively poor affinity, yielding low sensitivity in the assays employing them. Recently, single molecule recognition through equilibrium Poisson sampling (SiMREPS) has emerged as a platform for detecting proteins and other biomarkers with high sensitivity without requiring high-affinity detection probes. In this manuscript, we demonstrate the applicability and advantages of aptamers as detection probes in SiMREPS as applied to two clinically relevant biomarkers, $VEGF_{165}$ and IL-8, using a wash-free protocol with limits of detection in the low femtomolar range (3–9 fM). We show that the kinetics of existing RNA aptamers can be rationally optimized for use as SiMREPS detection probes by mutating a single nucleotide in the conserved binding region or by shortening the aptamer sequence. Finally, we demonstrate the detection of endogenous IL-8 from human serum at a concentration below the detection limit of commercial ELISAs.

1. Introduction

Proteins are useful biomarkers for differentiating between healthy and diseased states in clinical diagnostics (Simren et al., 2020). Sensitive and accurate quantification of proteins is the key for early-stage diagnosis of diseases. The long-standing gold-standard method for protein quantification in biofluids is the enzyme-linked immunosorbent assay (ELISA) (Engvall and Perlmann, 1971). However, the success of ELISA and its digital version (Rissin et al., 2010) in high-sensitivity applications depends on the so-called sandwich assay format, which imposes a nontrivial requirement of two antibodies that can simultaneously bind the same target protein at distinct epitopes with high affinity. In addition to batch-to batch variations in the production of antibody, it is tedious and challenging to generate specific, high affinity monoclonal antibodies, especially against non-immunogenic and toxic proteins (Toh et al., 2015). Moreover, these techniques cannot differentiate between specific signal from the protein of interest and non-specific signal from binding to assay surfaces or matrix (Chatterjee et al., 2020; Cohen and Walt, 2019).

A potential alternative to conventional antibody probes is provided by aptamers, synthetic single-stranded DNA (ssDNA) or RNA oligonucleotides that fold into unique three-dimensional structures and bind their targets specifically (Proske et al., 2005). Compared to antibodies, aptamers have several advantages. First, the generation of aptamers by systematic evolution of ligand by exponential enrichment (SELEX) can be performed faster and at lower cost than generating an antibody against a target protein by hybridoma or phage display technology (Gray et al., 2020; Tuerk and Gold, 1990). Moreover, solid-phase chemical synthesis permits aptamers to be synthesized more easily and more reproducibly than antibodies (Wang et al., 2011). Other advantages of aptamers include their non-toxicity and non-immunogenicity (Fish et al., 2003), reduced steric hindrance due to their smaller sizes (Lee et al., 2006), ease of modification, and thermal stability (Liss et al., 2002).

* Corresponding author.
** Corresponding author.
E-mail addresses: alex_johnson-buck@alightsci.com (A. Johnson-Buck), nwalter@umich.edu (N.G. Walter).

https://doi.org/10.1016/j.bios.2022.114639
Received 10 May 2022; Received in revised form 21 July 2022; Accepted 13 August 2022
Available online 22 August 2022

Due to the potential advantages of aptamers, ELISA-derived assays such as the-enzyme linked apta-sorbent assay (ELASA) have been developed (Drolet et al., 1996; Martin et al., 2013; Ramos et al., 2007; Zhang et al., 2018). However, these assays often have low sensitivity (limit of detection, LOD ~ 1 pM) and specificity (Toh et al., 2015; Zhang et al., 2018). To overcome this limitation, the SOMAscan assay utilizes modified aptamers called SOMAmers (slow off-rate modified aptamers) as recognition elements, permitting relatively high sensitivity and specificity in protein detection (median LOD for 1129 proteins ~ 40 fM) (Gold et al., 2010). However, this assay requires expensive synthetic nucleotide modifications, and, like conventional immunoassays, involves multistep sample handling procedures including stringent washing steps, and is unable to differentiate between specific and nonspecific binding (Gold et al., 2010; Rohloff et al., 2014).

Recently, Single Molecule Recognition through Equilibrium Poisson Sampling (SiMREPS) has emerged as a powerful technique for the ultrasensitive and specific detection of protein and other biomarkers, with LODs in the aM to low fM range (Chatterjee et al., 2020; Li et al., 2022; Mandal et al., 2021). The high sensitivity of SiMREPS results from its use of binding and dissociation kinetics to distinguish signal of specific binding to the target from that of nonspecific binding to the assay surfaces or matrix. To achieve this for proteins, a detection antibody with relatively fast dissociation kinetics (k_{off} ~0.05–0.5 s^{-1}) is needed to permit repeated interrogation of single target molecules and generate characteristic kinetic fingerprints within a reasonably short acquisition time (e.g., 2 min per field of view) without sacrificing sensitivity (Chatterjee et al., 2020).

Despite this success, there are several challenges associated with using antibodies as SiMREPS detection probes. While the success rate for generating protein-SiMREPS probes by phage display has been high, likely due to the relaxed affinity requirement compared to conventional immunoreagents (Chatterjee et al., 2020), developing recombinant antibody reagents by phage display nonetheless involves nontrivial time requirements and cost. While kinetics can be further manipulated using reaction conditions such as salt concentration or temperature (Chatterjee et al., 2020), it is difficult to rationally alter antibody sequences to achieve desired changes in binding or dissociation kinetics. Furthermore, antibodies often exhibit nonspecific adsorption to assay surfaces, even when passivated by reagents such as polyethylene glycol or Tween 20 (Hua et al., 2014). Although the kinetic analysis approach of SiMREPS allows one to filter out mild or moderate nonspecific binding, severe nonspecific binding can still interfere with the analysis and potentially exclude otherwise kinetically suitable antibodies from consideration (Chatterjee et al., 2020). Finally, fluorescent labeling of antibodies is typically performed in a non-regioselective manner (e.g., nonspecific labeling of lysine amines with *N*-hydroxysuccinimidyl ester reagents), and can result in loss of binding activity, increased kinetic heterogeneity, or aggregation of the antibody (McCormack et al., 1996; Vira et al., 2010).

Motivated by the advantages of aptamers as well as the tolerance of SiMREPS for lower-affinity detection probes than conventional immunoassays, in the present study we demonstrate the applicability of aptamers as detection probes in SiMREPS assays of two clinically relevant protein biomarkers: $VEGF_{165}$ and IL-8. We show that previously reported aptamers can be rationally optimized for use as dynamically binding SiMREPS probes by incorporating small sequence modifications during chemical synthesis, such as a single nucleotide substitution in the conserved region or the shortening of adjacent helical stems. Thus, unlike antibodies, aptamer sequences can be relatively easily modulated to achieve faster kinetics and, hence, faster data acquisition and better distinction between signal and background kinetic fingerprints. Furthermore, the use of chemical synthesis permits site-specific and stoichiometric fluorophore labelling of these aptamers at sites distal from the antigen-binding site, maintaining binding affinity as well as creating a simpler two-state fluorescence intensity behavior than nonspecifically labeled antibodies provide. Finally, we demonstrate the ultrasensitive detection of spiked-in $VEGF_{165}$ and endogenous human IL-8 in serum matrices using a wash-free protocol, yielding limits of detection in the low femtomolar range (3.1 fM or 0.026 pg/mL for IL-8 detection and 8.9 fM or 0.340 pg/mL for $VEGF_{165}$ detection).

2. Materials and methods

2.1. Oligonucleotides and proteins

All 2′-fluoropyrimidine-modified and 3′-Cy5-labelled RNA oligonucleotides were purchased from Integrated DNA Technologies (IDT, www.idtdna.com) with high-performance liquid chromatography (HPLC) purification. All oligonucleotide sequences are shown in Fig. 1D and Supporting Information Table S1. They were suspended in TE buffer (10 mM Tris, 0.1 mM EDTA, pH 8.0) to a final concentration of 100 μM and then aliquoted and stored at −80 °C. Recombinant human IL-8 (Ser28-Ser99, catalog# BR-1098) was provided in lyophilized form by Bio-Rad Laboratories, Inc. Biotinylated recombinant human IL-8 (catalogue # B-CXCL8-2 μg) was purchased from Chemotactics in lyophilized form. Recombinant human $VEGF_{165}$ was purchased from Abcam (catalogue # ab9571) as a lyophilized powder. Antigens were suspended in 1 × PBS, pH 7.4 (Gibco) supplemented with 10 mg/mL BSA (Thermo Scientific Blocker BSA (10x) in PBS; catalog No.- 37525) as a carrier, aliquoted, and frozen at −80 °C. Monoclonal IL-8 capture antibody (catalogue # EPR19358-108) and monoclonal $VEGF_{165}$ capture antibody (IgG) were purchased from Abcam and Bio-Rad Laboratories, respectively. The $VEGF_{165}$ capture antibody was provided as lyophilized powder from a 0.2 μm-filtered solution in PBS with 5% trehalose. Both of the capture antibodies were free of BSA and azide to facilitate labelling with biotin NHS ester. Horse serum (catalogue # H1270) and human serum (catalogue # H4522) were purchased from Sigma Aldrich.

2.2. Biotinylation of capture antibody

Monoclonal capture antibodies were biotinylated by amine-NHS ester coupling using biotin *N*-hydroxysuccinimidyl ester (Sigma Aldrich, Catalog # H1759-100) in reactions containing a molar biotin: antibody ratio of 5:1 which were carried out at room temperature for 1 h in 1 × PBS, pH 7.4. Biotin-IgG conjugates were purified using Zeba Spin desalting columns (ThermoFisher, Catalog # 89882, 7K MWCO) according to the manufacturer's recommended protocol, followed by overnight dialysis at 4 °C (Slide-A-Lyzer Dialysis Cassette, ThermoFisher, 3.5K MWCO) against 1 × PBS, pH 7.4. The fraction of biotinylated IgG was estimated by electrophoretic mobility shift assay in the presence or absence of excess streptavidin and ranged from 70% to 80%. Capture antibodies were aliquoted and frozen at −80 °C.

2.3. Preparation of slide surfaces for single-molecule microscopy

Glass coverslips (No. 1.5, 24 × 50 mm, VWR #48393–241) were functionalized with a 1:100 mixture of biotin-PEG-SVA and mPEG-SVA (Laysan Bio, Inc., #MPEG-SVA-5000-1g and #BIO-PEG-SVA-5K-100 MG) as previously described (Chatterjee et al., 2020). Coverslips were stored under aluminium foil in a nitrogen-purged cabinet until use (up to 4 weeks). Prior to an experiment, 2–6 sample cells were attached to each coverslip by cutting a ~2-cm length from the wider end of micropipette tips (Thermo Fisher, #02-682-261), discarding the narrower segment of the pipet tip, and then placing the wide end down on the PEGylated glass coverslip and then sealing the edges with epoxy adhesive (Ellsworth Adhesives, #4001).

2.4. TIRF microscopy

SiMREPS experiments were performed using Olympus IX-81 objective-type TIRF microscopes equipped with cellTIRF and z-drift control modules (ASI CRISP). Cy5 labelled detection aptamers were excited in

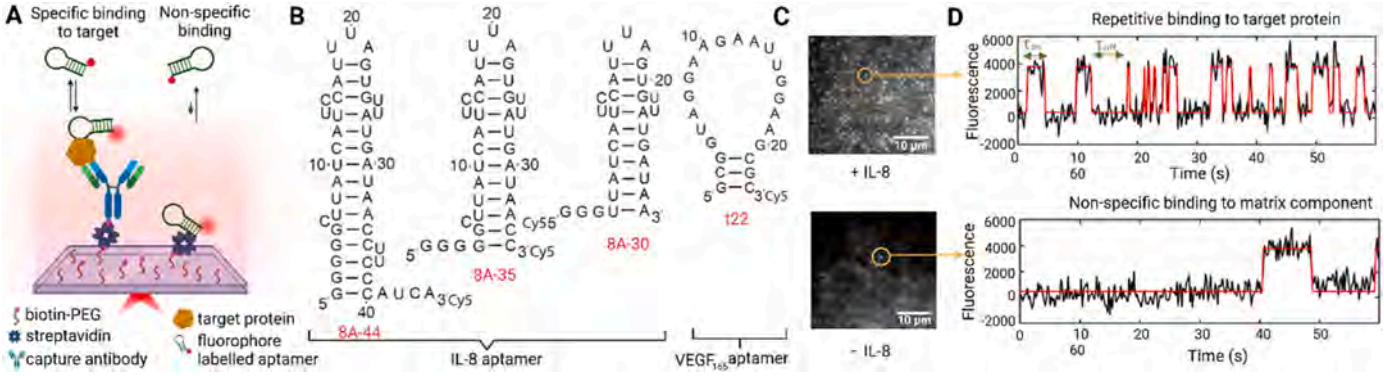

Fig. 1. Detection of single protein molecules by aptamer-based kinetic fingerprinting. (**A**) Experimental scheme for the detection of a target protein by aptamer-based SiMREPS. (**B**) Aptamers adopted from the literature with their sequences and secondary structures; IL-8 aptamers: 8A-44, 8A-35, 8A-30 and $VEGF_{165}$ aptamer t22. (**C**) Single movie frames of a representative microscope FOV; the bright puncta represent single fluorophore-labelled aptamers bound at or near the coverslip surface. The upper frame depicts a FOV from an experiment in the presence of recombinant IL-8 whereas the lower frame depicts a FOV from an experiment without IL-8. (**D**) Representative intensity-versus-time traces showing the distinct kinetic fingerprints of specific, repetitive binding to the target protein (top trace) and nonspecific binding to the assay surface (bottom trace).

TIRF mode with a theoretical penetration depth of ~80 nm using a fiber-coupled diode laser (OBIS 637 nm LX, 100 mW) with an incident light intensity of ~100 W/cm^2, and fluorescence emission was detected using an EMCCD (Photometrics Evolve) with an exposure time of 200 or 500 ms, after passing through a dichroic mirror and emission filter (ET655LP-TRF). In some experiments, an objective heater (Bioptechs) was used to raise the observation temperature to as high as 29 °C (calibrated against a reference thermistor provided by the manufacturer for the specific sample cell geometry used in this study).

2.5. Imaging solution

Unless otherwise specified, all SiMREPS assays were carried out in an imaging solution comprising 1 × PBS, pH 7.4 or 6 × PBS, pH 7.4 (Gibco); an oxygen scavenger system (Aitken et al., 2008) consisting of 5 mM 3, 4-dihydroxybenzoic acid (Fisher, #AC114891000), 0.05 mg/mL protocatechuate 3,4-dioxygenase (Sigma Aldrich, #P8279–25UN), and 1 mM Trolox (Fisher, #218940050); and 75–100 nM fluorophore-labelled detection aptamers.

2.6. SiMREPS assays of recombinant antigens

All sample handling was performed in GeneMate low-adhesion 1.7-mL microcentrifuge tubes, and dilutions were performed in 25% Horse serum, 0.75 × PBS, pH 7.4, and 7.5 mg/mL BSA. The slide surface was washed with 100 μL of T50 buffer (10 mM Tris-HCl, 50 mM NaCl, 1 mm EDTA, pH 8.0) for 10 minutes followed by the addition of 40 μL 1 mg/mL streptavidin. After 10 min, excess streptavidin was removed, and the sample chamber washed three times with 100 μL of 1 × PBS. Next, the coverslip was coated with the biotinylated capture antibody by adding 40 μL of a solution containing 10 nM of biotinylated capture antibody in 1 × PBS buffer and incubating for 30 min. Excess antibody was removed and the sample wells washed three times with 100 μL of 1 × PBS. A 100-μL portion of the antigen or blank solution was added to the sample chamber and incubated for 1 h to capture the antigen on the coverslip surface. The sample was removed, the sample cell washed twice with 100 μL of 1 × PBS, and 200 μL of imaging solution added. Kinetic fingerprints of aptamer binding were immediately imaged by TIRF microscopy using an acquisition time of 1 min–2 min per field of view (FOV) for IL-8 or 10 min per FOV for $VEGF_{165}$.

2.7. Wash-free SiMREPS standard curves

Capture antibody-coated glass coverslips were prepared as described above (Section 2.6.). A 200-μL volume of a mixture containing varying concentrations of recombinant human IL-8 and $VEGF_{165}$ spiked into 1% horse serum in 1 × PBS (IL-8 standard curve) or 6 × PBS ($VEGF_{165}$ standard curve), pH 7.4, containing 5 mM 3,4-dihydroxybenzoic acid, 0.05 mg/mL protocatechuate 3,4-dioxygenase, 1 mM Trolox, and 75 nM (IL-8 detection) or 100 nM ($VEGF_{165}$ detection) of fluorophore-labelled aptamer was added to the sample well and incubated for 40 min. Kinetic fingerprints of detection aptamer binding were then immediately imaged by TIRF microscopy using an acquisition time of 1 min per FOV at 24 °C for IL-8 detection and 5 min per FOV at 21 °C for $VEGF_{165}$ detection.

2.8. Wash-free measurement of endogenous IL-8 in human serum

Capture antibody-coated coverslips were prepared as described above (Section 2.6.). Samples of 2% and 10% human serum were prepared by adding 4 μL or 20 μL of human serum to a total volume of 200 μL imaging solution containing: 1 × PBS, pH 7.4, 5 mM 3,4-dihydroxybenzoic acid, 0.05 mg/mL protocatechuate 3,4-dioxygenase, 1 mM Trolox, and 75 nM of detection aptamer. This 200 μL mixture was added to the sample well and incubated for 40 min. Kinetic fingerprints of detection aptamer binding were then immediately imaged by TIRF microscopy using an acquisition time of 1 min per FOV at an acquisition temperature of 24 °C.

2.9. ELISA standard curves

Standard curves for detection of IL-8 from 100% human serum were performed using an IL-8 sandwich ELISA kit (Abcam, catalog # ab214030) according to the manufacturer's recommended protocol. The manufacturer's claimed LOD for the ELISA kit is 211 fM (1.8 pg/mL).

2.10. Analysis of SiMREPS data

SiMREPS data were analyzed using custom MATLAB code to identify sites of fluorophore labelled aptamer probe binding and analyze the kinetics of repeated binding as described previously using a diffraction-limited analysis pipeline (Johnson-Buck et al., 2019). Briefly, regions of repeated probe binding and dissociation (regions of interest, ROIs) in the FOV were identified by determining the average absolute frame-to-frame change in intensity at each pixel to create an intensity fluctuation map and then defining ROIs as the 3 × 3-pixel regions centered on local maxima within the fluctuation map. Next, the integrated, background-subtracted intensity within each ROI was calculated for each frame in the movie to generate an intensity-*versus*-time trace. These candidate traces were subjected to hidden Markov modeling

(HMM) using a version of vbFRET (Bronson et al., 2009). The idealized trace generated via HMM was used to determine several parameters for SiMREPS kinetic fingerprinting analysis: N_{b+d}, the number of binding and dissociation events; $\tau_{on,median}$ and $\tau_{off,median}$, the median dwell times in the probe-bound and probe-unbound states, respectively; $\tau_{off,max}$, the maximum dwell time in the probe-unbound state; and S/n, the signal-to-noise ratio, defined as the standard deviation of the fluorescence intensity divided by the mean intensity difference between bound and unbound states. Threshold values for each of these parameters to count a trace as a positive detection event were optimized heuristically for each probe-antigen pair.

3. Results and discussion

3.1. Aptamer based kinetic fingerprinting assay design

Our aptamer-based protein SiMREPS assays use two probes: a capture antibody, typically an IgG, with slow dissociation kinetics; and a low-affinity RNA aptamer with rapid dissociation kinetics (k_{off} ~0.05–0.5 s^{-1}) (Fig. 1A). The capture antibody is modified with biotin to permit surface immobilization of the target protein via a streptavidin bridge to a biotin-PEG (polyethylene glycol)-coated coverslip, while the aptamer is modified with an organic fluorophore either at the 3′ end or 5’ end to enable detection of its binding to the coverslip surface by total internal reflection fluorescence (TIRF) microscopy (Fig. 1A and B). As in their originally published form, the aptamers bear 2′-fluoro modifications at all pyrimidine nucleotides to increase the stability of the aptamers in serum (Ruckman et al., 1998; Sung et al., 2014). As in other immunoassays, we find that the fluorophore-labelled aptamers exhibit some nonspecific binding to assay surfaces, albeit at much lower levels than most fluorophore-labelled detection antibodies (Chatterjee et al., 2020), upon single molecule observation (Fig. 1C). In the absence of kinetic fingerprinting, this nonspecific binding would constitute background signal that could not be distinguished from specific binding. However, we find that the nonspecific binding typically exhibits kinetics of interaction quite distinct from the more repetitive specific binding of the detection aptamer to the target protein, making it readily distinguishable by analysis of localized fluorescence intensity fluctuations over time (Fig. 1D). Most notably, nonspecific interactions occur with much lower frequency at any given location on the surface, while the specific binding to the target protein generates repetitive binding at the same location (Fig. 1C and D). Thus by applying empirically determined thresholds that include a minimum number of binding (fluorescence-on transition) and dissociation (fluorescence-off transition) events (N_{b+d}) as well as minimum and maximum values of the median dwell time in the probe-bound state ($\tau_{on,median}$), we can distinguish single molecule traces arising from specific versus non-specific binding. Kinetic filtering thus helps to reduce false positive counts while keeping the majority of true positives, demonstrating the high specificity of aptamer based single molecule protein detection by kinetic fingerprinting. Significantly, in contrast to the multi-state intensity traces observed with inherently non-stoichiometrically labelled antibodies (Chatterjee et al., 2020), the single molecule time traces in the present study show two-state behavior since each copy of aptamer has (at most) one copy of active fluorophore (Fig. 1D). This simplifies the HMM fitting of the intensity-versus-time data and hence permits extraction of more accurate kinetic information for the digital counting of true positives.

3.2. Aptamer modification and assay optimization for $VEGF_{165}$ detection

For the detection of $VEGF_{165}$, we adopted aptamer t22 from the literature (Ruckman et al., 1998) (Fig. 1D). The aptamer was generated by SELEX from a randomized library of RNA sequences to bind $VEGF_{165}$ with high affinity and high specificity. Consistent with the expected specific binding of the aptamer to $VEGF_{165}$, our single-molecule fluorescence imaging revealed 8–10 times more fluorescent spots per FOV in the sample well containing $VEGF_{165}$ than in a control well without $VEGF_{165}$ (Fig. S1). However, consistent with the reported slow dissociation rate ($k_d \sim 0.012 \pm 0.0025\ s^{-1}$), stable binding of t22 probe to the surface captured $VEGF_{165}$ was observed in single molecule imaging, with lifetimes of several tens of seconds in the bound state. While useable, this dissociation rate is slower than ideal for a SiMREPS detection probe. This is because, in contrast to conventional detection probes, the best performance in SiMREPS is achieved not through high affinity for the analyte, but through observation of repeated interactions, which benefits from fast kinetics of binding and dissociation. Specifically, since the transient binding of the aptamer probe to a surface-immobilized protein target can be idealized as a Poisson process, the standard deviation in the number of binding and dissociation events (N_{b+d}) is expected to increase only as ($\sqrt{N_{b+d}}$), increasing the separation between specific and nonspecific kinetic signatures with increasing numbers of observed events. Thus to achieve high sensitivity and specificity in SiMREPS, it is helpful to have fast association (k_{on}) and dissociation (k_{off}) rate constants, which yield high N_{b+d} values in a shorter observation time. The most useful probes should exhibit k_{on} values of at least $0.5 \times 10^6\ M^{-1}\ s^{-1}$ and, with our typical time resolution, k_{off} values of 0.05–0.5 s^{-1}. Thus for a tightly binding probe like the t22 aptamer of VEGF165, N_{b+d} values are low, as the incumbent probe inhibits the binding of a new probe to the same analyte molecule. The relatively slow dissociation of t22 from the surface captured $VEGF_{165}$ thus makes it difficult to distinguish true and false positives on the basis of repeated binding (Fig. S2). However, after increasing the salt concentration 6-fold (from 1 × PBS to 6 × PBS), a subpopulation of traces in the sample well showed kinetics distinct from the blank well and could thus be labeled as true positives by applying appropriate kinetic filtering parameters (Fig. 2 D-E and Fig. S2). This influence of ionic strength suggests the involvement of ionic interactions between the probe and antigen. Raising the temperature yielded further increase in kinetics, but was not sufficient to separate the signal from the background completely (Fig. S3 and Fig. 2 D, E). To further improve performance, we screened five rationally designed mutations of t22 to evaluate their impact on kinetics (Fig. 2A and S4). Out of the mutations examined, a single G-to-A mutation in the conserved region of the t22 sequence (t22 G→A) yielded the greatest improvement in performance (Fig. 2A and B) due to its ~10-fold faster dissociation ($k_{off} = 0.22\ s^{-1}$ for t22 G→A vs $k_{off} = 0.02\ s^{-1}$ for t22) and ~2.3-fold faster association ($k_{on} = 5.1 \times 10^5\ M^{-1}s^{-1}$ for t22 G→A vs $k_{on} = 2.2 \times 10^5\ M^{-1}s^{-1}$ for t22) compared to the original t22 aptamer under identical buffer and imaging conditions (Fig. 2C). The increases in both dissociation and association rate accelerated the repeated binding of individual target molecules (Fig. 2B), increasing N_{b+d} and thus permitting substantially better resolution of specific from nonspecific kinetic behavior (Fig. 2F and G) (Johnson-Buck et al., 2015). We also attempted to further increase the k_{off} of the mutated aptamer (t22 G→A) by increasing the ionic strength of the buffer (from 6x PBS to 8x PBS) and temperature of the medium (from 21 °C to 28 °C). Increasing the ionic strength further causes little increase in the k_{off} value of the mutated aptamer but reduces the N_{b+d} value due to a decrease in association rate (k_{on}) (Fig. S5). On the other hand, increasing temperature to 28 °C has a negligible effect on the binding kinetics of the t22 G→A aptamer (Fig. S5). Thus, the assay of $VEGF_{165}$ by the t22 G→A aptamer appears to perform best at 6X PBS and 21 °C out of all conditions examined (Fig. S5). In conclusion, unlike with antibody probes, it is feasible to design site-specific nucleobase modifications by chemical synthesis to convert a stably binding aptamer to a lower-affinity SiMREPS probe showing rapid, repeated binding and dissociation.

3.3. Aptamer sourcing and assay optimization for IL-8 detection

The aptamers used for IL-8 detection in this study are shown in Fig. 1B. The parent aptamer 8A-W (91 nt) was generated in a previous

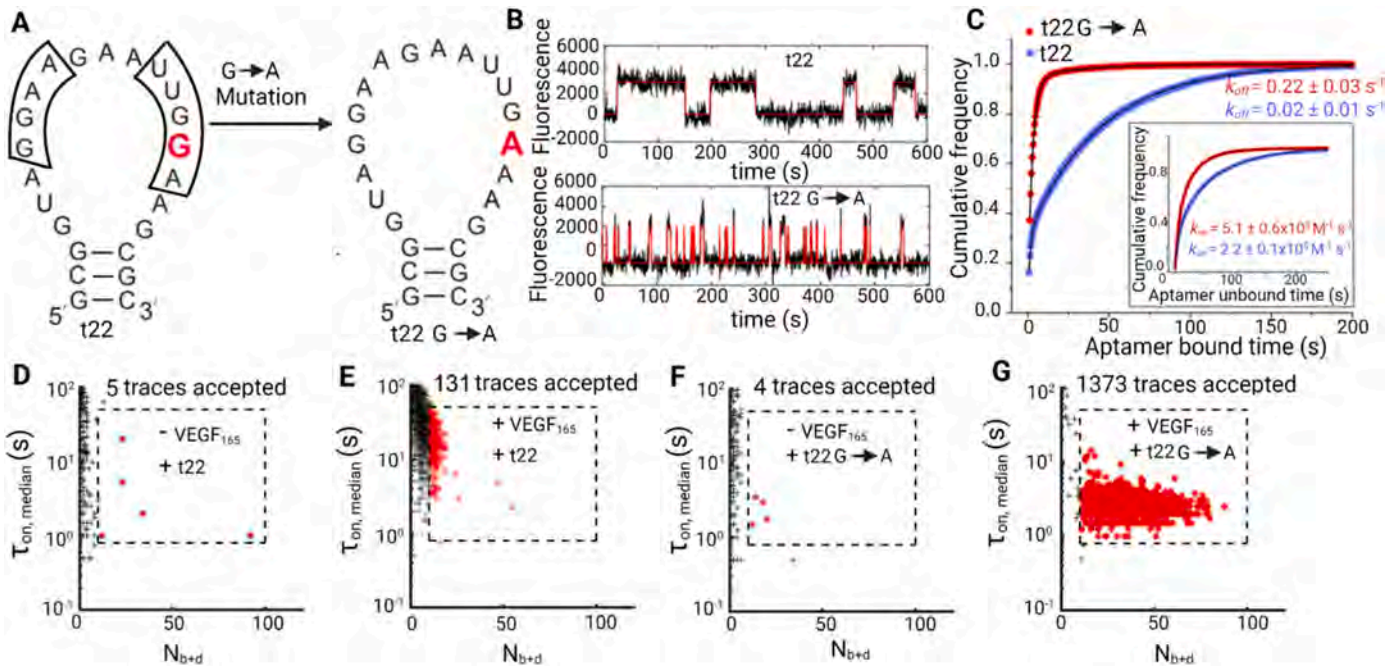

Fig. 2. Aptamer based detection of $VEGF_{165}$. (**A**) G-to-A mutation (Shown in red and bold-faced) in the conserved region (boxed) of the t22 aptamer results in the more rapidly dissociating t22 *G→A* aptamer. (**B**) Representative kinetic time traces of interaction of $VEGF_{165}$ with the t22 aptamer (upper trace) and the t22 *G→ A* aptamer (lower trace). (**C**) Cumulative bound and unbound (inset) dwell time histograms of the Cy5-labelled t22 aptamer (blue squares) and t22 *G→ A* aptamer (red circles). The overall binding (k_{on}) and dissociation (k_{off}) rate constants of interaction between $VEGF_{165}$ and t22 or between $VEGF_{165}$ and t22 *G→ A* are indicated. The reported errors are the standard error of the mean from two independent replicates. (**D, E, F, G**) Scatterplots of N_{b+d} and $\tau_{on,median}$ for all intensity-versus-time trajectories observed within a single field of view in the absence (**D, F**) and in the presence (**E, G**) of 5 pM $VEGF_{165}$ (10 minutes acquisition time, 500 ms exposure, 1200 frames). (**D**) and (**E**) depict the kinetics of the original t22 aptamer, while (**F**) and (**G**) depict the kinetics of the modified t22 *G→A* aptamer. The dashed lines indicate the minimum and maximum thresholds for accepting a trace as evidence of a single $VEGF_{165}$ molecule. "+" symbols represent traces that do not pass filtering for intensity, signal-to-noise, and/or kinetics and are rejected as detection events of $VEGF_{165}$; red filled circles represent traces that pass filtering and are considered positive detection events.

report by the SELEX method against human IL-8 and was then truncated to generate 8A-44 (44 nt, 14.6 kDa), 8A-35 (35 nt, 11.8 kDa) and 8A-30 (30 nt, 10.1 kDa), without compromising binding to IL-8 (Sung et al., 2014). We hypothesized that the more truncated versions of these aptamers might perform better as SiMREPS probes because previous reports show that smaller probes often have better access to the epitope on the target protein, especially when a small protein is immobilized by a capture antibody (Dey et al., 2005; Lee et al., 2006). To systematically assess the effect of aptamer size on the kinetics of binding to the small (8.4 kDa) protein IL-8, we employed two different antigen capture strategies: direct capture, in which C-terminally biotin-labelled IL-8 was immobilized directly on the surface by the biotin-streptavidin interaction; and antibody-mediated capture, in which non-biotinylated IL-8 was captured on the surface by a surface-immobilized biotinylated monoclonal antibody (Fig. 3A). Kinetic time trajectories of single IL-8 molecules interacting with the various Cy5-labelled aptamers show that binding and dissociation kinetics are systematically influenced by both aptamer truncation and the capture strategy (Fig. S6). To gain more quantitative insight, association and dissociation rate constants were calculated from the dwell time distributions in the aptamer-unbound and -bound states, respectively, and are shown in Table 1.

In direct capture, all the aptamer variants show similar dissociation rates ($k_{off} \sim 0.5\ s^{-1}$) (Fig. 3B), but their association rates decrease from $5.68 \times 10^6\ M^{-1}\ s^{-1}$ to $2.08 \times 10^6\ M^{-1}\ s^{-1}$ as the aptamer size increases (Fig. 3C). This inverse relationship between size and binding rate may result in part from the slower diffusion coefficient *D* of the probe with increasing molecular weight *M*; however, the expected relationship $D \propto \frac{1}{\sqrt{M}}$ (Grushka and Kikta, 1976) would only account for a ~1.2-fold change in binding kinetics, suggesting that other factors such as reduced productivity of collisions may be playing a role. In antibody-mediated capture, the dissociation rate from the IL-8 binding site increases for all the aptamers, albeit to different degrees (Fig. 3D). The dissociation rate is fastest for 8A-44 ($k_{off} \sim 2.5\ s^{-1}$) and slowest for 8A-30 ($k_{off} \sim 1.17\ s^{-1}$), suggesting that steric hindrance between the antibody and larger aptamers may be accelerating dissociation. Furthermore, antibody-mediated capture reduces the association rates of all the aptamers, but by the greatest factor for the larger aptamers 8A-44 and 8A-35; for the short 8A-30 aptamer, the association rate only decreases by a factor of ~1.2 (Fig. 3E). The fast binding and dissociation of 8A–30 results in a higher number of binding/dissociation events (N_{b+d}) within a given observation period and, hence, better separation between signal and background kinetics, than 8A-35 or 8A-44 (Fig. 3F and G and Supp. Info. Fig. S7). This shows that the performance of an aptamer in SiMREPS can be improved by truncating non-conserved portions of the sequence, resulting in faster kinetics and therefore more rapid data acquisition and/or higher analytical performance. Such optimizations are difficult or impossible for antibody probes, which have a relatively fixed overall structure that cannot be easily modified. Due to its fast kinetics, 8A-30 was chosen for further use and optimization in SiMREPS assays of IL-8 in serum (Fig. 3H and I). As an additional optimization, we found that slightly raising temperature from 21 °C to 24 °C further increases the kinetics of 8A–30, permitting a data acquisition time of only 1 min per field of view without compromising signal/background discrimination (Fig. 3H, I and Fig. S8). Further increasing to 27–29 °C did not result in significant improvements relative to 24 °C.

3.4. Analytical performance and detection of endogenous IL-8 in human serum

To investigate the sensitivity and specificity of aptamer-based SiMREPS protein assays, human $VEGF_{165}$ and IL-8 were spiked into horse

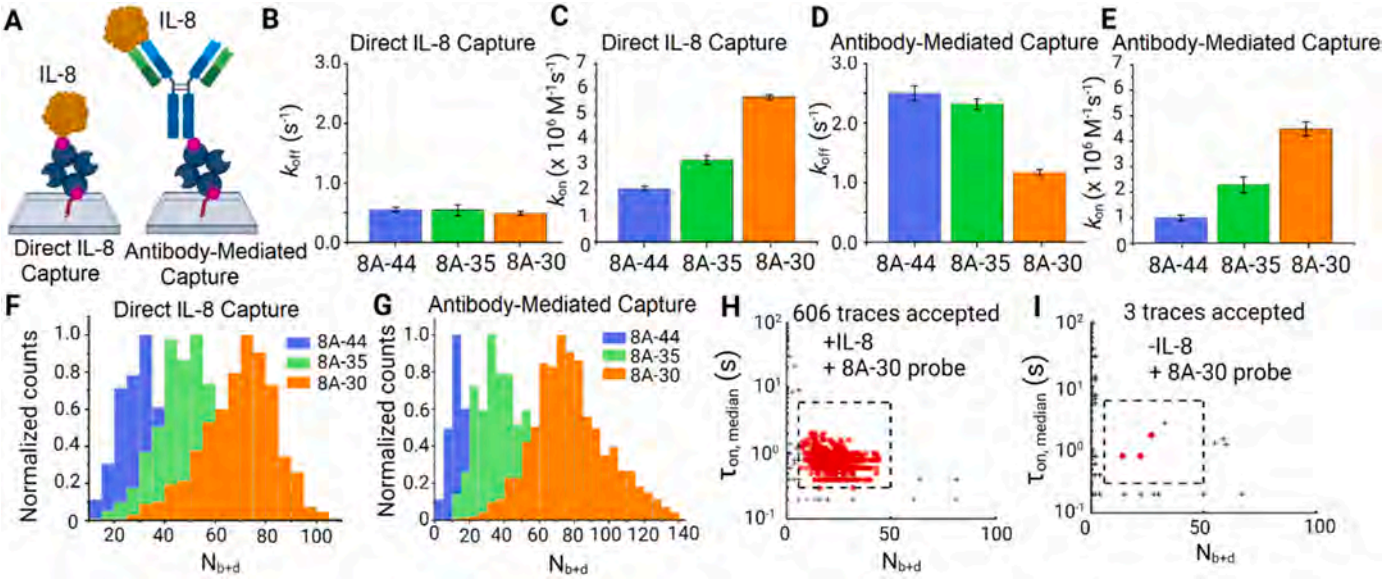

Fig. 3. Characterization of aptamer probes for IL-8. (**A**) Schematic depiction of two capture strategies for IL-8: direct capture of C-terminally biotinylated IL-8 to streptavidin; and antibody-mediated capture of non-biotinylated IL-8. (**B, C**) Dissociation rate constants (**B**) and association rate constants (**C**) of Cy5 labelled aptamers (8A-44, 8A-35 and 8A-30) interacting with directly captured biotinylated IL-8 as measured by TIRF microscopy. (**D, E**) Dissociation rate constants (**D**) and association rate constants (**E**) of Cy5-labelled aptamers interacting with antibody-captured IL-8. Error bars represents the standard error of the mean from two independent replicates. (**F, G**) Normalized histograms of the number of intensity transitions per single-molecule trace arising from aptamer binding or dissociation (N_{b+d}) of Cy5-labelled aptamers interacting with directly captured biotinylated IL-8 (**F**) or antibody-captured IL-8 (**G**) with a 5-min acquisition time at 21 °C. H, I Scatterplots of N_{b+d} and $\tau_{on,median}$ for all intensity-versus-time trajectories observed within a single field of view in the presence (**H**) and in the absence (**I**) of 1 pM IL-8 (1 min acquisition time at 24 °C). Dashed lines indicate thresholds for accepting a trace as evidence of a single IL-8 molecule. Points indicated by "+" represent traces that do not pass filtering for intensity, signal-to-noise, and/or kinetics and are not considered as interactions between IL-8 and 8A-30 aptamer. Points indicated by red filled circles represent traces that pass filtering and are considered positive detection events.

Table 1
Binding parameters arising from interaction between Cy5-labelled 8A aptamers (at 75 nM) and IL-8 in 25% horse serum at 21 °C as determined by single-molecule fluorescence microscopy.

Capture strategy	Aptamer	k_{on} x 10^{-6} ($M^{-1}s^{-1}$)	k_{off} (s^{-1})	K_D (μM)
Direct IL-8 capture	8A-44	2.08 ± 0.12	0.55 ± 0.04	0.264 ± 0.061
	8A-35	3.21 ± 0.18	0.54 ± 0.09	0.168 ± 0.032
	8A-30	5.68 ± 0.09	0.50 ± 0.04	0.088 ± 0.010
Antibody mediated capture	8A-44	0.99 ± 0.11	2.50 ± 0.13	2.52 ± 0.074
	8A-35	2.29 ± 0.32	2.32 ± 0.09	1.01 ± 0.089
	8A-30	4.48 ± 0.28	1.17 ± 0.05	0.261 ± 0.018

serum at varying concentrations and then measured by SiMREPS using our nuclease-resistant 2′-fluoropyrimidine-modified RNA aptamers. These assays were performed using a wash-free protocol wherein serum samples with spiked in protein was simply mixed with imaging buffer, added to a capture-antibody-coated coverslip surface, and then imaged after a suitable incubation period (Fig. 4A). Hence, unlike in conventional assays, neither the sample nor the excess detection probe need to be washed away after sample addition. The acquisition parameters and kinetic filtering criteria for the quantification of $VEGF_{165}$ and IL-8 are shown in the Supplementary Information (Table S2). As shown in Fig. 4B and C, the aptamer probes detect IL-8 and $VEGF_{165}$ spiked into serum with very low background, and the signal exhibits a linear dependence upon target protein concentration. The fact that wash-free experiments in serum yield low background signal suggests that any interference from the complex mixture of biomolecules in a serum matrix can be largely or completely overcome by kinetic filtering in SiMREPS (Fig. S9). The estimated LODs are 3.1 fM (0.026 pg/mL) for IL-8 and 8.9 fM (0.34 pg/mL) for $VEGF_{165}$, demonstrating high sensitivity for both targets. The same assays performed with the original, unmodified aptamers (t22 and 8A-44) show much lower sensitivity (~7-fold higher LOD for VEGF165 and ~16-fold higher LOD for IL-8) than the corresponding mutated/truncated aptamers under identical experimental conditions, supporting the effectiveness of the chosen aptamer modifications for highly sensitive detection of proteins by SiMREPS assays (Fig. S10). The lower sensitivity of the unmodified aptamers is mainly due to the less complete separation between signal and background (due to slower kinetics) that results in higher false positive counts in blank measurements. We have also found that the high sensitivity of aptamer based SiMREPS allowed detection of IL-8 from as low as 1:50 diluted (2%) human serum (0.035 pg/mL IL-8, corresponding to 1.75 pg/mL IL-8 in the original serum sample) while the corresponding sandwich ELISA failed to detect IL-8 even at in undiluted (100%) human serum, showing that aptamer-based SiMREPS can detect analytes too dilute to assay by conventional methods (Fig. 4D and E).

4. Conclusions

In this study, we have demonstrated the applicability of fluorophore-labelled aptamers as rationally tunable probes for the highly sensitive and specific detection of two clinically relevant protein biomarkers, $VEGF_{165}$ and IL-8, by SiMREPS. As with previously reported protein-SiMREPS assays using Fab antibody detection probes (Chatterjee et al., 2020), aptamer-based SiMREPS achieves low-femtomolar (sub-pg/mL) LODs in animal and human serum, exceeding the sensitivity of commercial ELISAs by more than two orders of magnitude, and can be performed using a wash-free protocol that bypasses the tedious multi-step washing protocols required of most immunoassays. However, as we have shown here, aptamers possess several advantages as SiMREPS probes compared to antibodies, including the ability to rationally

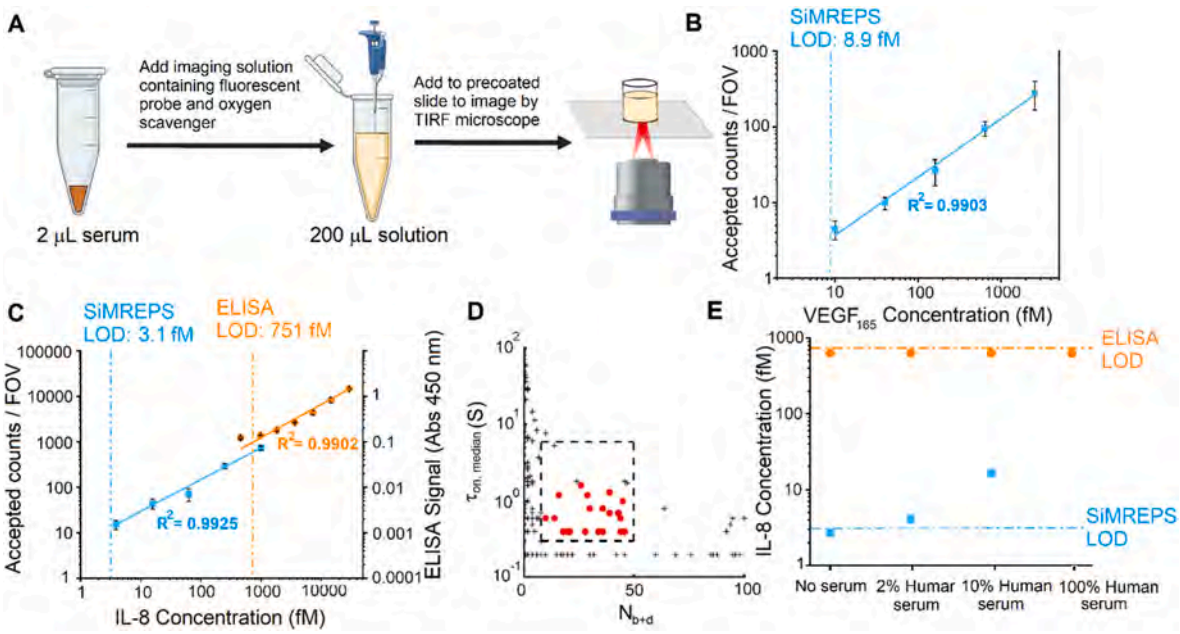

Fig. 4. Wash-free assays of spiked-in and endogenous protein targets. (**A**) Wash-free SiMREPS protocol for quantifying IL-8 and $VEGF_{165}$ in serum. A serum sample containing spiked-in or endogenous IL-8 or $VEGF_{165}$ is combined with the imaging solution and then added to a capture antibody-coated coverslip. After a suitable incubation period (40 min), the sample is imaged by TIRF microscopy to quantify IL-8 and $VEGF_{165}$. (**B, C**) Standard curves showing quantification of spiked-in $VEGF_{165}$ (**B**) or IL-8 (**C**) using aptamer-based SiMREPS (blue squares) or sandwich ELISA (orange circles). Linear regression fits are shown as blue (SiMREPS) or orange (sandwich ELISA) solid lines. Error bars indicate the SD of three independent measurements. (**D**) Scatterplots of N_{b+d} and $\tau_{on,median}$ for all intensity-versus-time trajectories observed within a single field of view for the detection of endogenous IL-8 from 2% Human serum at 24 °C. (**E**) SiMREPS detects IL-8 in 2% and 10% Human serum (blue square); by contrast, a commercial ELISA (orange circle) cannot detect IL-8 even in undiluted (100%) Human serum.

tune their kinetics of interaction with the target through selective mutation or truncation, and the ease of introducing site-specific and stoichiometric fluorophore modifications using chemical synthesis. These features have direct impact on their use as SiMREPS probes by influencing the required data acquisition time (faster kinetics result in faster data collection) and complexity of intensity-versus time traces (two-state intensity behavior is simpler to analyze than multi-state behavior). Aptamers are also simpler to generate, cheaper to synthesize, and—if nuclease-resistant nucleotides are used as was done here—more tolerant of varied storage conditions than antibodies. Importantly, the aptamers examined in this study showed even less nonspecific binding to assay surfaces and matrix proteins than most antibody probes examined previously.

We have shown two kinds of rational modification of aptamer sequences to improve their performance as SiMREPS probes: reduction in affinity of tightly binding probes using single-nucleotide changes in the conserved target-binding region, and increasing binding kinetics by truncating sequence not directly involved in the interaction. We only needed a very limited number of trials (<10) to optimize the design. Given that aptamers suitable to such rapid rational redesign are available from SELEX approaches against over 1000 human proteins (Brody et al., 2012; Gold et al., 2010; Hathout et al., 2015; Thanasupawat et al., 2021), our assay can be readily adapted to many biomarkers of disease. In addition, as with antibody probes (Chatterjee et al., 2020), binding and/or dissociation rates can be increased by elevating the temperature or by manipulating the ionic strength of the solution, resulting in improved assay performance or reduced measurement time. Thus, although antibody detection probes for SIMREPS are readily generated by phage display, the addition of aptamers as detection probes provides more paths to generating probes with the desired rapid binding and dissociation kinetics, and therefore is expected to drastically facilitate the development of high-performance assays against a wide range of targets important in research and diagnostics.

CRediT authorship contribution statement

Tanmay Chatterjee: Conceptualization, Investigation, Writing – original draft, Writing – review & editing, Visualization, Validation, Formal analysis, Methodology. **Alexander Johnson-Buck:** Conceptualization, Writing – review & editing, Software, Supervision. **Nils G. Walter:** Conceptualization, Supervision, Funding acquisition, Writing – review & editing.

Declaration of competing interest

The authors declare the following financial interests/personal relationships which may be considered as potential competing interests: N.G.W and A.J.-B are cofounder of aLight Sciences, Inc., which seeks to commercialize the SiMREPS technology. A.J.-B is an employee of aLight Sciences, Inc.; N.G.W and A.J.-B are co-inventors of patent applications related to the SiMREPS technology.

Data availability

Data will be made available on request.

Acknowledgements

This work was funded by aLight Sciences, Inc. Antibodies ($VEGF_{165}$ monoclonal antibody) and recombinant antigens (human IL-8) were provided by Bio-Rad Laboratories, Inc. SiMREPS analysis software was developed in part using funding from a Michigan Economic Development Corporation MTRAC for Life Sciences grant to N.G.W. and A.J-B, as well as NIH grants R21 CA204560 and R33 CA229023 to N.G.W.

Appendix A. Supplementary data

Supplementary data to this article can be found online at https://doi.org/10.1016/j.bios.2022.114639.

References

Aitken, C.E., Marshall, R.A., Puglisi, J.D., 2008. An oxygen scavenging system for improvement of dye stability in single-molecule fluorescence experiments. Biophys J 94 (5), 1826–1835.

Brody, E., Gold, L., Mehan, M., Ostroff, R., Rohloff, J., Walker, J., Zichi, D., 2012. Life's simple measures: unlocking the proteome. J Mol Biol 422 (5), 595–606.

Bronson, J.E., Fei, J.Y., Hofman, J.M., Gonzalez, R.L., Wiggins, C.H., 2009. Learning rates and states from biophysical time series: a bayesian approach to model selection and single-molecule fret data. Biophys J 97 (12), 3196–3205.

Chatterjee, T., Knappik, A., Sandford, E., Tewari, M., Choi, S.W., Strong, W.B., Thrush, E. P., Oh, K.J., Liu, N., Walter, N.G., Johnson-Buck, A., 2020. Direct kinetic fingerprinting and digital counting of single protein molecules. P Natl Acad Sci USA 117 (37), 22815–22822.

Cohen, L., Walt, D.R., 2019. Highly sensitive and multiplexed protein measurements. Chem Rev 119 (1), 293–321.

Dey, A.K., Khati, M., Tang, M., Wyatt, R., Lea, S.M., James, W., 2005. An aptamer that neutralizes R5 strains of human immunodeficiency virus type 1 blocks gp120-CCR5 interaction. J Virol 79 (21), 13806–13810.

Drolet, D.W., MoonMcDermott, L., Romig, T.S., 1996. An enzyme-linked oligonucleotide assay. Nat Biotechnol 14 (8), 1021–1025.

Engvall, E., Perlmann, P., 1971. Enzyme-linked immunosorbent assay (elisa) quantitative assay of immunoglobulin-G. Immunochemistry 8 (9), 871–&.

Fish, G., Haller, J.A., Ho, A.C., Klein, M., Loewenstein, J., Martin, D., Orth, D., Rosen, R. B., Sanislo, S., Schwartz, S.D., Singerman, L.J., Williams, G., Adamis, A.P., Blumenkranz, M., Goldberg, M., Gragoudas, E.S., Miller, J.W., Yannuzzi, L., Guyer, D.R., O'Shaughnessy, D., Patel, S., Grp, E.S., 2003. Anti-vascular endothelial growth factor therapy for subfoveal choroidal neovascularization secondary to age-related macular degeneration - phase II study results. Ophthalmology 110 (5), 979–986.

Gold, L., Ayers, D., Bertino, J., Bock, C., Bock, A., Brody, E.N., Carter, J., Dalby, A.B., Eaton, B.E., Fitzwater, T., Flather, D., Forbes, A., Foreman, T., Fowler, C., Gawande, B., Goss, M., Gunn, M., Gupta, S., Halladay, D., Heil, J., Heilig, J., Hicke, B., Husar, G., Janjic, J., Jarvis, T., Jennings, S., Katilius, E., Keeney, T.R., Kim, N., Koch, T.H., Kraemer, S., Kroiss, L., Le, N., Levine, D., Lindsey, W., Lollo, B., Mayfield, W., Mehan, M., Mehler, R., Nelson, S.K., Nelson, M., Nieuwlandt, D., Nikrad, M., Ochsner, U., Ostroff, R.M., Otis, M., Parker, T., Pietrasiewicz, S., Resnicow, D.I., Rohloff, J., Sanders, G., Sattin, S., Schneider, D., Singer, B., Stanton, M., Sterkel, A., Stewart, A., Stratford, S., Vaught, J.D., Vrkljan, M., Walker, J.J., Watrobka, M., Waugh, S., Weiss, A., Wilcox, S.K., Wolfson, A., Wolk, S. K., Zhang, C., Zichi, D., 2010. Aptamer-based multiplexed proteomic technology for biomarker discovery. Plos One 5 (12).

Gray, A., Bradbury, A.R.M., Knappik, A., Pluckthun, A., Borrebaeck, C.A.K., Dubel, S., 2020. Animal-free alternatives and the antibody iceberg. Nat Biotechnol 38 (11), 1234–1239.

Grushka, E., Kikta, E.J., 1976. Diffusion in liquids .2. Dependence of diffusion-coefficients on molecular-weight and on temperature. J Am Chem Soc 98 (3), 643–648.

Hathout, Y., Brody, E., Clemens, P.R., Cripe, L., DeLisle, R.K., Furlong, P., Gordish-Dressman, H., Hache, L., Henricson, E., Hoffman, E.P., Kobayashi, Y.M., Lorts, A., Mah, J.K., McDonald, C., Mehler, B., Nelson, S., Nikrad, M., Singer, B., Steele, F., Sterling, D., Sweeney, H.L., Williams, S., Gold, L., 2015. Large-scale serum protein biomarker discovery in Duchenne muscular dystrophy. Proc Natl Acad Sci U S A 112 (23), 7153–7158.

Hua, B.Y., Han, K.Y., Zhou, R.B., Kim, H.J., Shi, X.H., Abeysirigunawardena, S.C., Jain, A., Singh, D., Aggarwal, V., Woodson, S.A., Ha, T., 2014. An improved surface passivation method for single-molecule studies. Nat Methods 11 (12), 1233–+.

Johnson-Buck, A., Li, J.M., Tewari, M., Walter, N.G., 2019. A guide to nucleic acid detection by single-molecule kinetic fingerprinting. Methods 153, 3–12.

Johnson-Buck, A., Su, X., Giraldez, M.D., Zhao, M.P., Tewari, M., Walter, N.G., 2015. Kinetic fingerprinting to identify and count single nucleic acids. Nat Biotechnol 33 (7), 730–732.

Lee, J.F., Stovall, G.M., Ellington, A.D., 2006. Aptamer therapeutics advance. Curr Opin Chem Biol 10 (3), 282–289.

Li, Z., McNeely, M., Sandford, E., Tewari, M., Johnson-Buck, A., Walter, N.G., 2022. Attomolar sensitivity in single biomarker counting upon aqueous two-phase surface enrichment. ACS Sens.

Liss, M., Petersen, B., Wolf, H., Prohaska, E., 2002. An aptamer-based quartz crystal protein biosensor. Anal Chem 74 (17), 4488–4495.

Mandal, S., Li, Z., Chatterjee, T., Khanna, K., Montoya, K., Dai, L., Petersen, C., Li, L., Tewari, M., Johnson-Buck, A., Walter, N.G., 2021. Direct kinetic fingerprinting for high-accuracy single-molecule counting of diverse disease biomarkers. Acc Chem Res 54 (2), 388–402.

Martin, M.E., Garcia-Hernandez, M., Garcia-Recio, E.M., Gomez-Chacon, G.F., Sanchez-Lopez, M., Gonzalez, V.M., 2013. DNA aptamers selectively target leishmania infantum H2A protein. Plos One 8 (10).

McCormack, T., OKeeffe, G., MacCraith, B., OKennedy, R., 1996. Assessment of the effect of increased fluorophore labelling on the binding ability of an antibody. Anal Lett 29 (6), 953–968.

Proske, D., Blank, M., Buhmann, R., Resch, A., 2005. Aptamers - basic research, drug development, and clinical applications. Appl Microbiol Biot 69 (4), 367–374.

Ramos, E., Pineiro, D., Soto, M., Abanades, D.R., Martin, M.E., Salinas, M., Gonzalez, V. M., 2007. A DNA aptamer population specifically detects Leishmania infantum H2A antigen. Lab Invest 87 (5), 409–416.

Rissin, D.M., Kan, C.W., Campbell, T.G., Howes, S.C., Fournier, D.R., Song, L., Piech, T., Patel, P.P., Chang, L., Rivnak, A.J., Ferrell, E.P., Randall, J.D., Provuncher, G.K., Walt, D.R., Duffy, D.C., 2010. Single-molecule enzyme-linked immunosorbent assay detects serum proteins at subfemtomolar concentrations. Nat Biotechnol 28 (6), 595–599.

Rohloff, J.C., Gelinas, A.D., Jarvis, T.C., Ochsner, U.A., Schneider, D.J., Gold, L., Janjic, N., 2014. Nucleic acid ligands with protein-like side chains: modified aptamers and their use as diagnostic and therapeutic agents. Mol Ther-Nucl Acids 3.

Ruckman, J., Green, L.S., Beeson, J., Waugh, S., Gillette, W.L., Henninger, D.D., Claesson-Welsh, L., Janjic, N., 1998. 2 '-fluoropyrimidine RNA-based aptamers to the 165-amino acid form of vascular endothelial growth factor (VEGF(165)) - inhibition of receptor binding and VEGF-induced vascular permeability through interactions requiring the exon 7-encoded domain. J Biol Chem 273 (32), 20556–20567.

Simren, J., Ashton, N.J., Blennow, K., Zetterberg, H., 2020. An update on fluid biomarkers for neurodegenerative diseases: recent success and challenges ahead. Curr Opin Neurobiol 61, 29–39.

Sung, H.J., Choi, S., Lee, J.W., Ok, C.Y., Bae, Y.S., Kim, Y.H., Lee, W., Heo, K., Kim, I.H., 2014. Inhibition of human neutrophil activity by an RNA aptamer bound to interleukin-8. Biomaterials 35 (1), 578–589.

Thanasupawat, T., Glogowska, A., Pascoe, C., Krishnan, S.N., Munir, M., Begum, F., Beiko, J., Krcek, J., Del Bigio, M.R., Pitz, M., Shen, Y., Spicer, V., Coombs, K.M., Wilkins, J., Hombach-Klonisch, S., Klonisch, T., 2021. Slow off-rate modified aptamer (SOMAmer) proteomic analysis of patient-derived malignant glioma identifies distinct cellular proteomes. Int J Mol Sci 22 (17).

Toh, S.Y., Citartan, M., Gopinath, S.C.B., Tang, T.H., 2015. Aptamers as a replacement for antibodies in enzyme-linked immunosorbent assay. Biosens Bioelectron 64, 392–403.

Tuerk, C., Gold, L., 1990. Systematic evolution of ligands by exponential enrichment - rna ligands to bacteriophage-T4 DNA-polymerase. Science 249 (4968), 505–510.

Vira, S., Mekhedov, E., Humphrey, G., Blank, P.S., 2010. Fluorescent-labeled antibodies: balancing functionality and degree of labeling. Anal Biochem 402 (2), 146–150.

Wang, P., Yang, Y., Hong, H., Zhang, Y., Cai, W., Fang, D., 2011. Aptamers as therapeutics in cardiovascular diseases. Curr Med Chem 18 (27), 4169–4174.

Zhang, W.L., He, Z.Y., Yi, L.L., Mao, S.F., Li, H.F., Lin, J.M., 2018. A dual-functional microfluidic chip for on-line detection of interleukin-8 based on rolling circle amplification. Biosens Bioelectron 102, 652–660.

Supplementary Information for

Highly Sensitive Protein Detection by Aptamer-Based Single-Molecule Kinetic Fingerprinting

Tanmay Chatterjee[a], Alexander Johnson-Buck[b*], and Nils G. Walter[a*]

[a]Single Molecule Analysis Group, Department of Chemistry, University of Michigan, Ann Arbor, Michigan 48109, United States

[b]aLight Sciences, Inc., 333 Jackson Plaza Suite 460, Ann Arbor, Michigan 48103, United States

Email:

*Corresponding author: nwalter@umich.edu

*Corresponding author: alex_johnson-buck@alightsci.com

Table of Contents

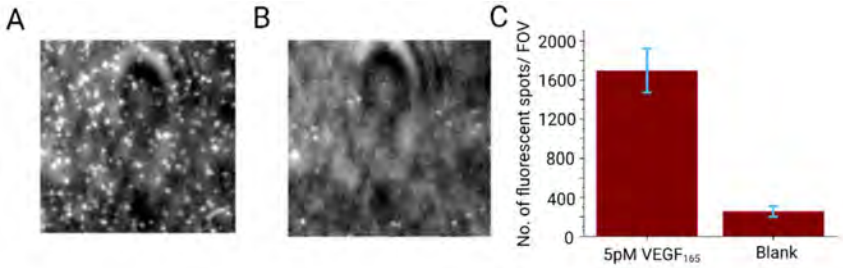

Figure S1. Fluorescent spot density of t22 aptamer in presence and absence of $VEGF_{165}$. Single field of view showing fluorescent spots density on the surface in presence of 5 pM $VEGF_{165}$ (A) and in absence of $VEGF_{165}$ (B). The number of fluorescent spots is ~8-10 times higher in the sample well containing $VEGF_{165}$ than the control well without $VEGF_{165}$ under identical buffer (1X PBS containing 100 nM Cy5 labelled t22 aptamer) and imaging condition (C). Intensity threshold for fluorescent spot counting is $I_{threshold}$ = 600 and signal to noise ratio, S/N = 2.

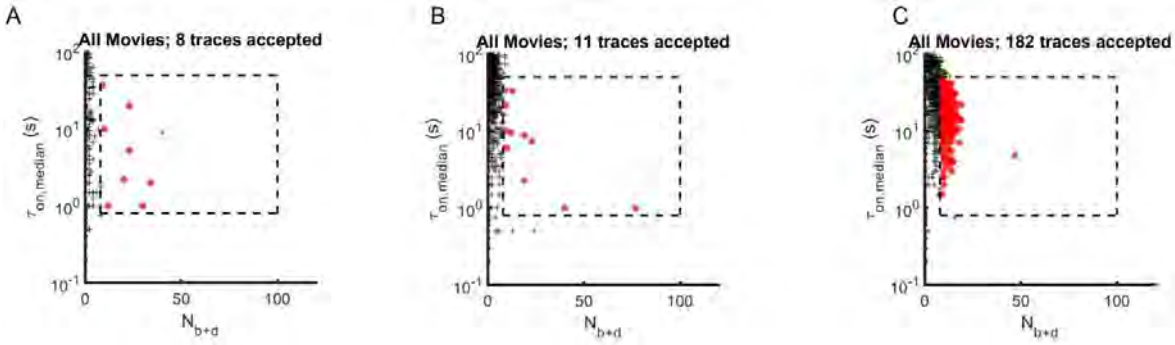

Figure S2: Effect of Salt concentration on the binding kinetics of t22 aptamer to $VEGF_{165}$. Scatter plots of N_{b+d} and $\tau_{on,median}$ for all intensity-versus-time trajectories observed within a single field of view in the absence of $VEGF_{165}$(A) and in the presence (B , C) of 5 pM VEGF165. The imaging solution for A and B contains 1x PBS and that of C contains 6x PBS. Points indicated by "+" represent traces that do not pass filtering for intensity, signal-to-noise, and/or kinetics and are not classified as arising from interaction between $VEGF_{165}$ and aptamers. Points indicated by red filled circles represent traces that pass filtering and are considered positive detection events.

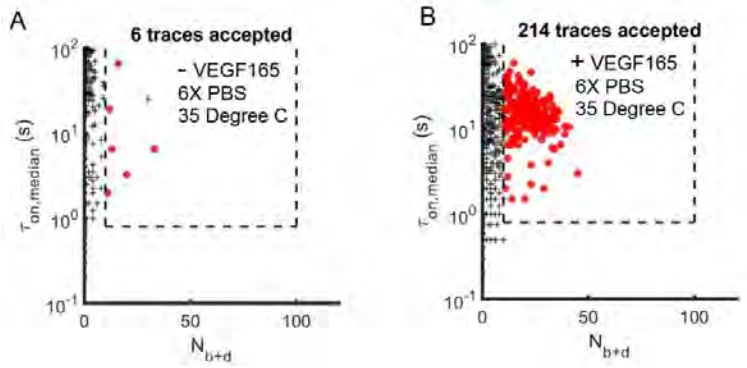

Figure S3: Influence of both temperature and ionic strength on the interaction of t22 aptamer to $VEGF_{165}$. Scatter plots of N_{b+d} and $\tau_{on,median}$ for all intensity-versus-time trajectories observed within a single field of view in the absence of $VEGF_{165}$(A) and in the presence (B) of 60 pM biotinylated VEGF165. The imaging solution for A and B contains 6x PBS and the data were collected at 36 °C. Points indicated by "+" represent traces that do not pass filtering for intensity, signal-to-noise, and/or kinetics and are not considered as interaction between VEGF-165 and aptamers. Points indicated by red filled circles represent traces that pass filtering and are considered positive detection events.

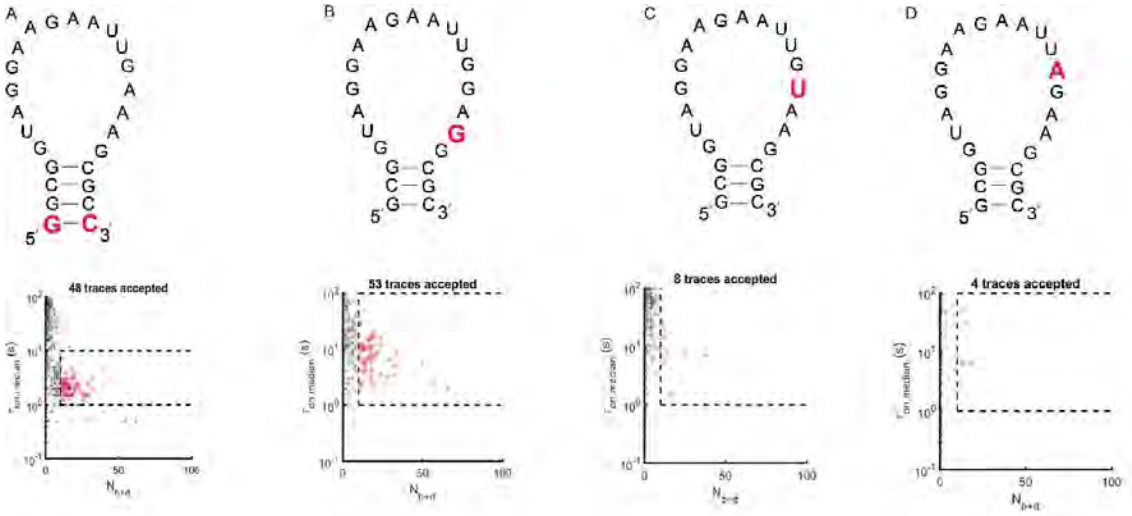

Figure S4: Effect of aptamer modification on binding to $VEGF_{165}$. Modified aptamers of t22 (A-D). The mutated bases are shown in bold red color. The respective lower panel shows scatter plots of N_{b+d} and $\tau_{on,median}$ for all intensity-versus-time trajectories observed within a single field of view in the presence of 5 pM $VEGF_{165}$ in 6x PBS at room temperature. While the modified aptamers shown in figure A, B and C still interacts with $VEGF_{165}$. Mutation of G to A in position shown in figure D completely abolish interaction with $VEGF_{165}$.

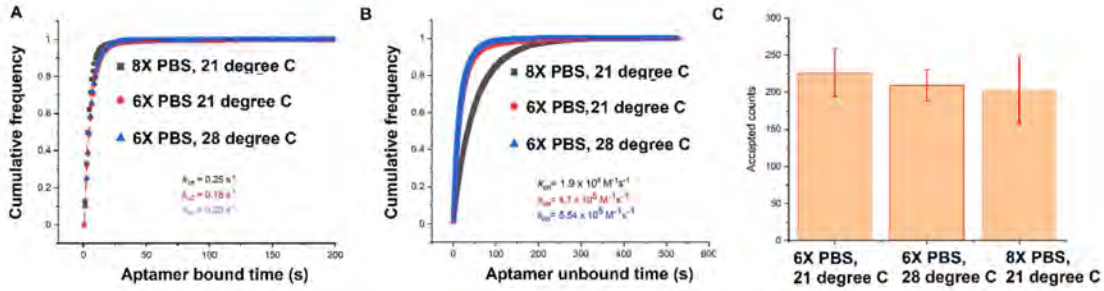

Figure S5: Effect of increasing ionic strength and temperature on binding kinetics and assay performance of t22 G→A aptamer. Binding and dissociation assay of t22 G →A aptamer under varying ionic strength and temperature. (A ,B) Cumulative bound (A) and unbound (B) dwell time histograms of the Cy5-labelled t22 $G \rightarrow A$ aptamer (8X PBS - black squares; 6X PBS - red circles; 6X PBS at 28 °C – blue triangles). The overall binding (k_{on}) and dissociation (k_{off}) rate constants of interaction between $VEGF_{165}$ and t22 $G \rightarrow A$ aptamer are indicated. (C) Variation in accepted counts/ FOV for the detection of 2.56 pM $VEGF_{165}$ by t22 $G \rightarrow A$ aptamer under varying conditions.

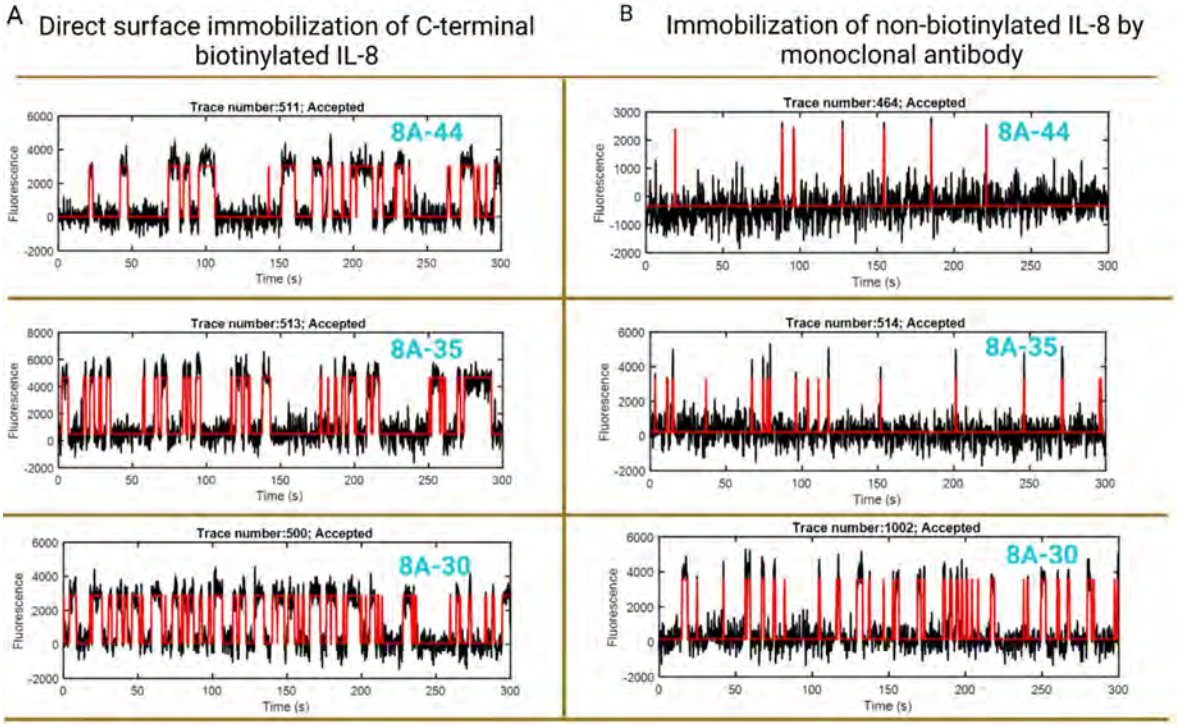

Figure S6: Representative kinetic time traces showing interaction of 8A aptamers with IL-8. (A) The interaction of 8A aptamers with directly surface captured biotinylated IL-8. (B) Interactions of 8A aptamers with monoclonal antibody captured IL-8.

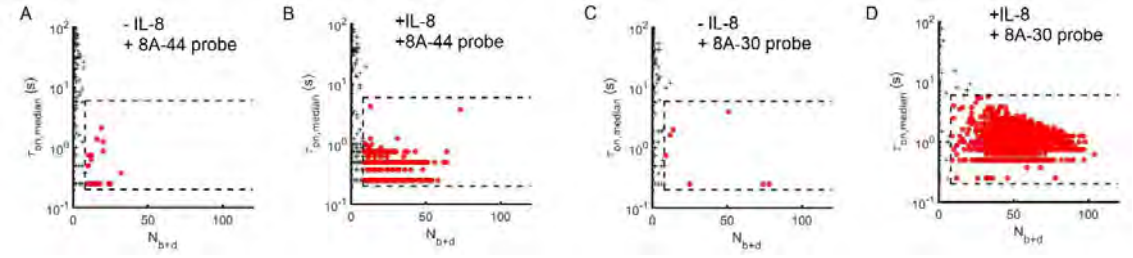

Figure S7: Effect of probe length (8A-30 and 8A-44 aptamer) on SiMREPS assay performance. Scatter plots of N_{b+d} and $\tau_{on,median}$ for all intensity-versus-time trajectories observed within a single field of view in the absence of IL-8 (A and C) and in the presence of 10 pM IL-8 (B and D) in 25% Horse serum using a 2 min acquisition time at 24 °C. A and B represent experiments done with the 8A-44 probe; C and D represent experiments done with the 8A-30 probe. Dashed lines indicate thresholds for accepting a trace as evidence of a single IL-8 molecule. Points indicated by "+" represent traces that do not pass filtering for intensity, signal-to-noise, and/or kinetics and are not classified as interactions between IL-8 and 8A aptamers. Points indicated by red filled circles represent traces that pass filtering and are classified as positive detection events.

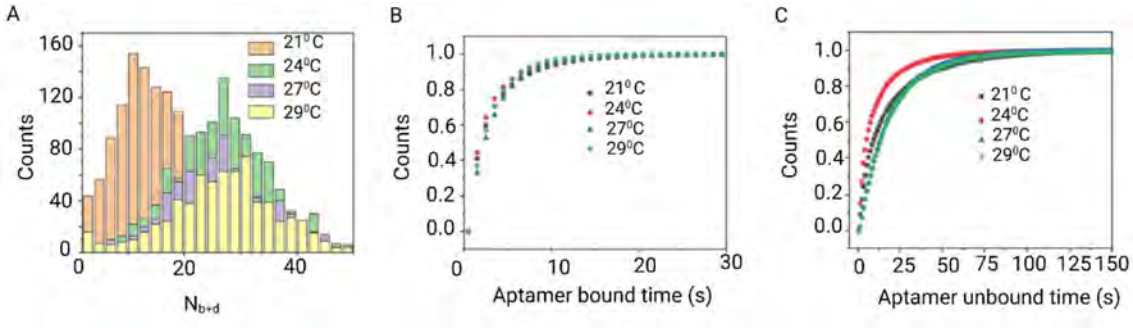

Figure S8: Influence of temperature on the interaction kinetics of 8A-30 aptamer with IL-8. (A) The peak of the N_{b+d} distribution shifts towards higher values by increasing the temperature from 21 °C to 24 °C. A further increase in temperature does not further affect the peak. (B) The aptamer bound time and hence the dissociation rates are similar at different temperatures. (C) The association rate increases with an increase in temperature from 21 °C to 24 °C. However, increasing the temperature further to 27 °C only changes the shape of the cumulative distribution curve.

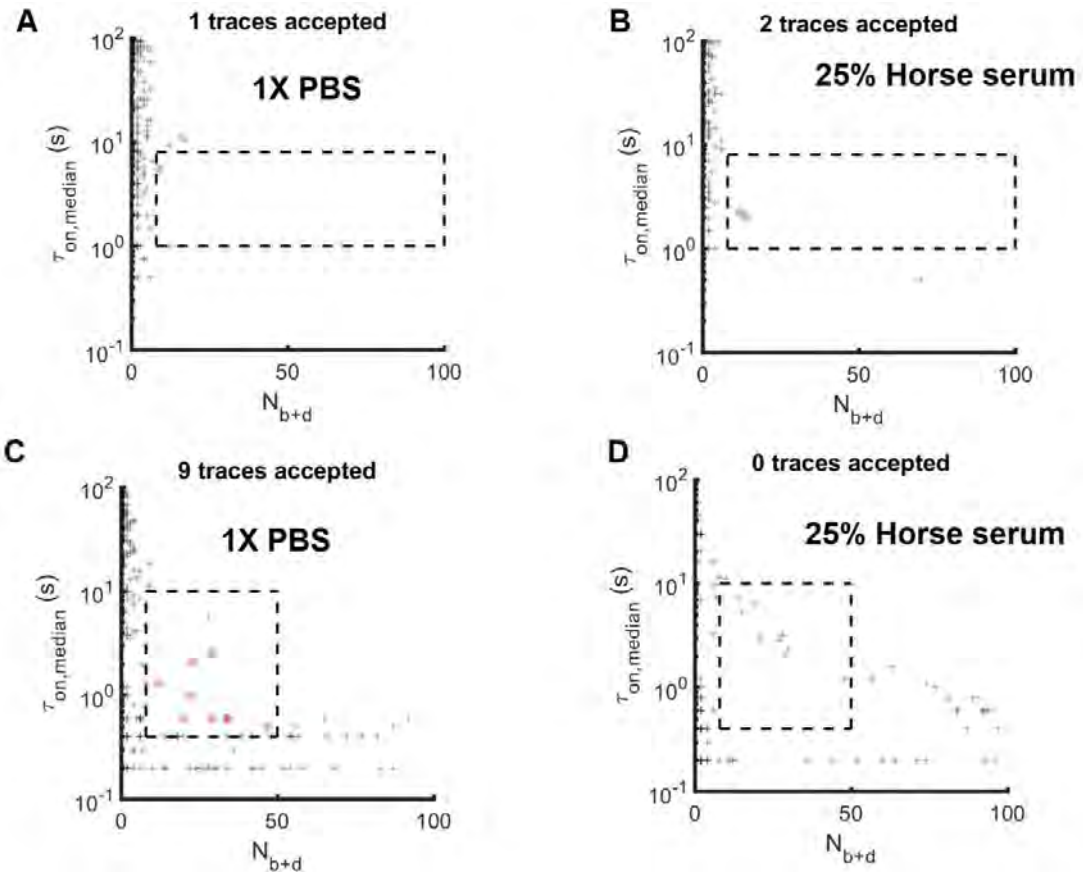

Figure S9: Background signal and kinetic filtering in 25% horse serum matrix under wash free condition. Scatter plots of N_{b+d} and $\tau_{on,median}$ for all intensity-versus-time trajectories observed within a single field of view in 1X PBS (A) and in Horse serum (B) without spiked-in $VEGF_{165}$. Scatter plots of N_{b+d} and $\tau_{on,median}$ for all intensity-versus-time trajectories observed within a single field of view in 1X PBS (C) and in Horse serum (D) without spiked-in IL-8 . The aptamer used for experiment (A and B) is t22 G→A and 8A-30 for IL-8 (C and D). Dashed lines indicate thresholds for accepting a trace as evidence of a single protein molecule. Points indicated by "+" represent traces that do not pass filtering for intensity, signal-to-noise, and/or kinetics and are not considered as interactions between VEGF165 and t22 G→A aptamer (A, B) and IL-8 and 8A-30 aptamer (C, D). Points indicated by red filled circles represent traces that pass filtering and are considered positive detection events.

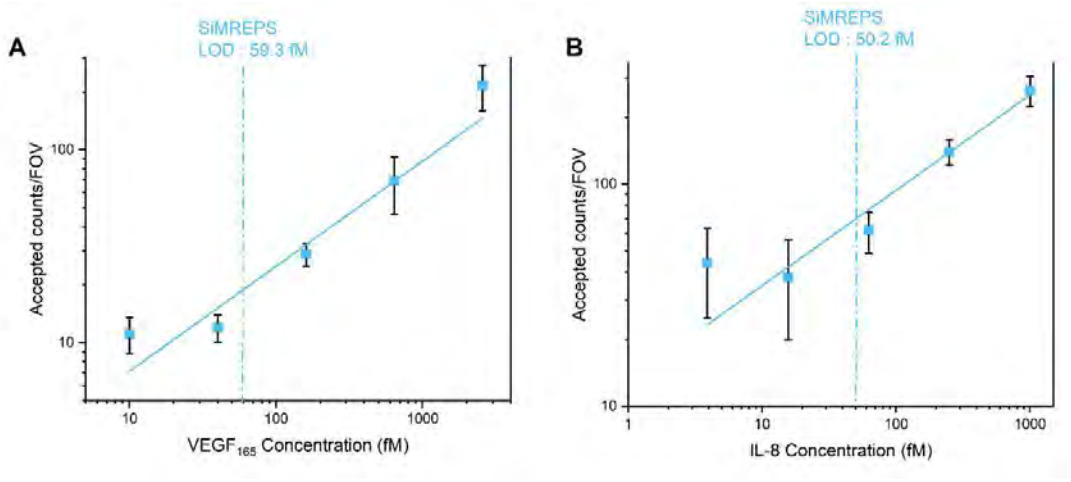

Figure S10: Limit of detection (LOD) calculation for $VEGF_{165}$ and IL-8 quantification using original aptamers (t22 and 8A-44). Standard curves showing quantification of spiked-in $VEGF_{165}$ (A) and IL-8 (B) in 25% Horse serum under wash free condition using t22 and 8A-44 aptamers respectively. Linear regression fits are shown as blue solid lines. Error bars indicates standard deviation of the mean from three independent experiments.

Supplementary Table S1: Oligonucleotide Sequences of 2´-fluoropyrimidine-modified RNA aptamers.

Modified RNA Aptamers	Aptamer sequences with nucleobase modifications (IDT, www.idtdna.com)
8A-44	5´GGGGG/i2FC//i2FU//i2FU/A/i2FU//i2FC/A/i2FU//i2FU//i2FC//i2FC/A/i2FU//i2FU//i2FU/AG/i2FU/G/i2FU//i2FU/A/i2FU/GA/i2FU/AA/i2FC//i2FC//i2FU/UCCCAUCA 3´Cy5
8A-35	5´GGGGG/i2FC//i2FU//i2FU/A/i2FU//i2FC/A/i2FU//i2FU//i2FC//i2FC/A/i2FU//i2FU//i2FU/AG/i2FU/G/i2FU//i2FU/A/i2FU/GA/i2FU/AA/i2FC//i2FC// 3´Cy5
8A-30	5´Cy5/GGG/i2FU//i2FU/A/i2FU//i2FC/A/i2FU//i2FU//i2FC//i2FC/A/i2FU//i2FU//i2FU/AG/i2FU/G/i2FU//i2FU/A/i2FU/GA/i2FU/AA
t22	5´G/i2FC/GG/i2FU/AGGAAGAA/i2FU//i2FU/GGAAG/i2FC/G/i2FC// 3´Cy5

Supplementary Table S2: Acquisition parameters and kinetic filtering criteria for optimized SiMREPS assays of each antigen.

	IL-8	$VEGF_{165}$
Detection probe	Aptamer 8A-30	Aptamer t22 G→A
Detection probe concentration (nM)	75	100
Exposure time per frame (s)	0.2	0.5
Acquisition time (min)	1	5
Acquisition temperature (°C)	24	21
Minimum $r_{s/n}$ per event	2	2
Minimum $r_{s/n}$ per trace	2	3
Minimum N_{b+d}	8	5
Maximum N_{b+d}	50	100
Minimum $\tau_{on,median}$ (s)	0.25	1
Maximum $\tau_{on,median}$ (s)	2	5.5
Minimum $\tau_{off,median}$ (s)	0.8	2
Maximum $\tau_{off,median}$ (s)	50	200